Lisandro Leon[1]
Department of Mechanical Engineering,
University of Utah,
Salt Lake City, UT 84112
e-mail: l.leon@utah.edu

Matt S. Cavilla
Department of Mechanical Engineering,
University of Utah,
Salt Lake City, UT 84112
e-mail: matt.cavilla@utah.edu

Michael B. Doran
Department of Mechanical Engineering,
University of Utah,
Salt Lake City, UT 84112
e-mail: mike.doran@utah.edu

Frank M. Warren
Department of Otolaryngology,
Division of Otology and Skull Base Surgery,
Oregon Health & Science University,
Portland, OR 97239
e-mail: warrenf@ohsu.edu

Jake J. Abbott
Department of Mechanical Engineering,
University of Utah,
Salt Lake City, UT 84112
e-mail: jake.abbott@utah.edu

Scala-Tympani Phantom With Cochleostomy and Round-Window Openings for Cochlear-Implant Insertion Experiments

Experiments with scala-tympani (ST) phantoms are used to evaluate new electrode arrays and cochlear-implant insertion techniques. To date, phantoms have not accounted for clinical orientations and geometric differences between round-window (RW) insertions and anteroinferior cochleostomy insertions. For improved assessments of insertion experiments, we present a scala-tympani phantom that offers three distinct benefits over previous phantoms: it mimics the standard otologic position, it accommodates for both round-window and anteroinferior cochleostomy insertions, and it incorporates a visual coordinate system based on industry consensus making standardized angular measurements possible. [DOI: 10.1115/1.4027617]

1 Introduction

A cochlear implant (CI) is an array of electrodes that is surgically inserted into the ST chamber of the cochlea to partially restore hearing. Ongoing interest in atraumatic CI insertions has prompted numerous electrode-array designs and insertion techniques. A common method for evaluating the effectiveness of these novel designs and strategies is through insertion force experiments in an ST phantom, especially in the early stages of development, where the added cost and complexity of using temporal bones or in vivo experiments are not yet warranted.

Although many phantoms with varying levels of fidelity have been used [1–8], to date, there has not been one designed specifically to model the realistic surgical constraints present in clinical practice imposed upon CI insertions. Typical phantom openings do not model the geometries of the RW or an anteroinferior cochleostomy, which are the openings used in actual insertions. Orienting typical phantoms so that insertion experiments duplicate clinically realistic angles (Fig. 1) require data on the cochlea's orientation which, until now, has not been synthesized into one convenient source. Although Advanced Bionics (Valencia, CA) provides a base that will orient their cochlea phantom appropriately, they make no claims regarding its accuracy. Current phantoms have also not addressed recent industry consensus for a standardized coordinate system in response to the challenges of interpreting results from various investigators [9]. We address these concerns with an ST phantom designed for improved cochlear-implant insertion experiments.

2 Standard Otologic Position

CI surgery is performed in the conventional otologic position, with the patient's back flat on the operating table, and the head turned toward the side by approximately 65 deg. This orients the skull such that the angle between the operating table and the skull's midsagittal plane is approximately 25 deg (Fig. 1). If necessary, the table is further adjusted to provide an optimal view into the cochlea to perform the surgery.

The primary difficulty in orienting a phantom to mimic this standard position is that the orientation of the cochlea within the skull or with respect to specific landmarks on the body is not readily available. One group [10–12] interested in using standard radiographic techniques to determine the postoperative position of a CI's electrode bands inside the cochlea determined the required skull orientation relative to a central X-ray beam (Fig. 2) necessary to produce an optimized 2D radiograph of the cochlea (Fig. 3) in which the plane of the basal cochlear turn (and the electrode array) is essentially parallel to the film plane. This method, known as the cochlear view (CV), requires the X-ray beam to be parallel to the modiolar axis (the central spiral axis of the cochlea) and orthogonal to the basal turn. This has become the standard 2D radiologic view of the cochlea [13], with some regarding it as the optimal 2D view of the cochlea [9]. Their work effectively defined the spatial orientation of the cochlea inside the skull, which we adopt to orient the ST phantom with respect to a tabletop.

The three angles with respect to anatomic landmarks required to orient the cochlea are shown in Figs. 2 and 3 and summarized in Table 1. The first two angles (θ_1 and θ_2) orient the cochlear axis relative to the skull's midsagittal plane and infraorbitomeatal plane, respectively. The third angle (θ_3) locates the RW in the plane through the basal turn. Unlike the first two angles, which are given relative to anatomic landmarks, the third angle can be difficult to visualize since it is given with respect to an abstract reference (0 deg reference in Fig. 3).

To understand this abstract reference with respect to an anatomical landmark, we examine Fig. 4, which shows a detailed version of Fig. 2(*a*). The modiolar axis, the plane of the superior-semicircular canal (SSC), and the X-ray are nearly parallel, making the film plane nearly orthogonal to all three. Since the X-ray is

[1]Corresponding author.

Manuscript received January 7, 2014; final manuscript received May 1, 2014; published online August 19, 2014. Assoc. Editor: Rafael V. Davalos.

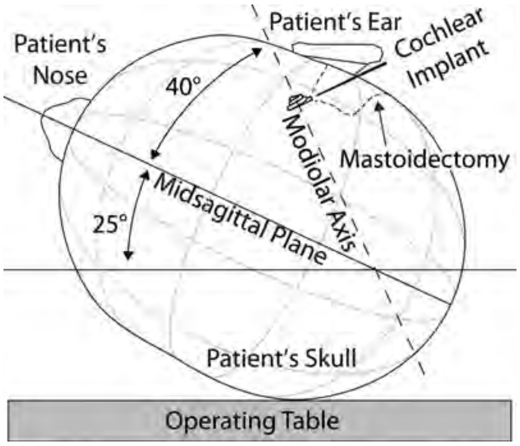

Fig. 1 Diagram of the standard otologic positioning

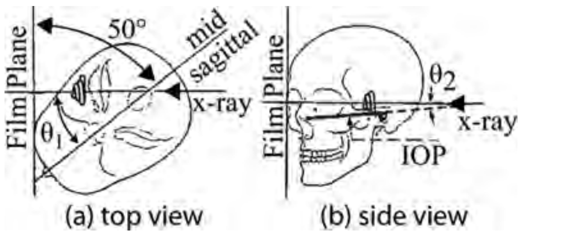

Fig. 2 The method to generate the cochlear view of Fig. 3 is summarized. (*a*) While the X-ray and film plane are maintained orthogonal to each other, the skull is positioned against the film such that the angle between it and the midsagittal plane is approximately 50 deg. (*b*) Next, the skull is adjusted so that the angle between the X-ray and the infraorbitomeatal plane (IOP) is near zero. Upon completion, the modiolar axis is nearly parallel to the X-ray. Modified image from Ref. [10] reproduced with permission of Wolters Kluwer Health.

parallel to the plane of the SSC, the SSC appears as a single structure [10]. Otherwise, it would appear as an elliptical loop similar to the view of the lateral-semicircular canal in Fig. 3. The line cv_2 in Fig. 3 drawn from the apex of the SSC through the center of the vestibule will lie in both the planes of the SSC and the film plane. The line cv_1 is drawn in the film plane orthogonal to cv_2, and by extension, must be orthogonal to the plane of the SSC.

The vertex view of Fig. 4 implies that the line-of-sight and the SSC plane are orthogonal to any transverse plane of the body (Fig. 5). Since θ_1 is neither 0 deg nor 90 deg, the SSC plane is never orthogonal to the coronal or sagittal planes. Therefore, cv_1 must lie on a transverse plane. This is convenient given that the infraorbitomeatal plane (sometimes referred to as the skull's horizontal plane [12]) can also be reasonably assumed to be parallel with any transverse plane. θ_3 can then be regarded as the angle between the infraorbitomeatal plane and the RW in the plane of the film (i.e., the plane of the basal cochlear turn), providing the anatomic landmark by which to interpret θ_3.

Since we are interested in orienting a phantom relative to a tabletop as in Fig. 1, the cochlear orientation relative to anatomic landmarks must be converted into angles relative to the operating table. The solution is as simple as implementing a series of coordinate frame rotations (Fig. 5). First, we assume the patient's back lies flat on an operating table whose surface is parallel with all coronal planes and orthogonal to all sagittal and transverse planes. Next, we define a cochlear Cartesian frame consisting of three orthogonal vectors that are initially aligned with the superior, lateral, and anterior vectors. The orientation of the modiolar axis is identical to the orientation of the anterior axis after the cochlear frame has been initially rotated by $-\theta_1$ about the superior axis

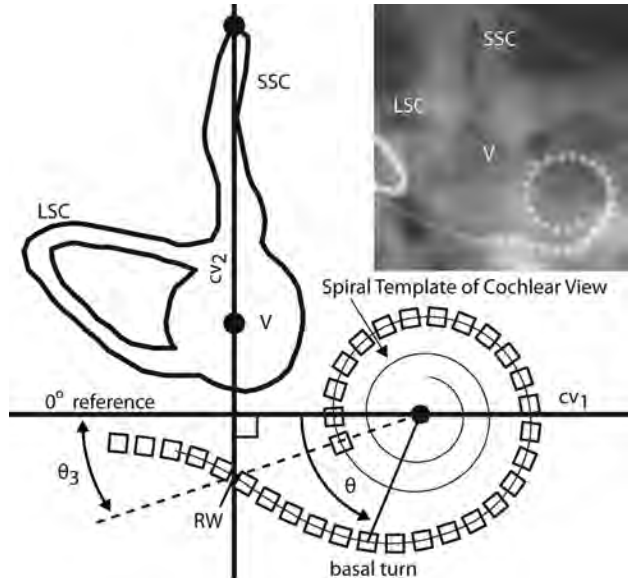

Fig. 3 The skull positioning of Fig. 2 results in the cochlear view, which contains a 2D image of the electrode array (shown as a series of squares) as a nonoverlapping spiral in the basal and middle turns. The spiral center is determined by fitting a mathematical spiral template to the position of the electrodes. The line cv_2 passes through the top of SSC and the midpoint of the vestibule (V). The line cv_1 passes through the spiral center and is orthogonal to cv_2. Angular insertion depth (θ) is measured from the geometric 0 deg reference, which is the line from the spiral center through the intersection of cv_1 and cv_2. The location of the RW entry, which is near the intersection of cv_2 and the electrode array, is measured from the 0 deg reference and shown here as θ_3. LSC is the lateral-semicircular canal. Modified image from Ref. [12] reproduced with permission of Wolters Kluwer Health.

Table 1 Cochlea orientation with respect to anatomic landmarks

Description	References	Value
θ_1 between midsagittal plane	[10]	40 deg
and spiral axis of the cochlea	[12]	37.5 deg (range of 15.5 deg)
θ_2 between infraorbitomeatal plane	[10]	0 deg
and spiral axis of the cochlea	[12]	1.8 deg (range of 6 deg)
θ_3 locates round window in the	[11]	13.47 deg
plane of basal turn	[9,14]	13.5 deg (range of 12.4 deg)

(Fig. 5(*a*)) followed by a rotation of $+\theta_2$ about the new lateral axis (Fig. 5(*b*)). The 0 deg reference in Fig. 3 is identical to this new lateral axis. The location of the RW is located on the final lateral axis after rotation by $+\theta_3$ about the final anterior axis (Fig. 5(*c*)). The modiolar axis orientation relative to a tabletop surface as in Fig. 1 requires a final rotation of the cochlear frame by +65 deg about the original superior axis (not shown).

3 Insertion Openings

Access to the ST for CI insertions are typically achieved through an incision in the RW membrane or through a cochleostomy sited anteroinferior to the RW on the cochlear promontory. The actual RW opening is typically sited on the vertical segment of the RW membrane (situated anteroinferiorly) rather than its horizontal segment (located posterosuperiorly) [16]. This is shown in the lower-left inset of Fig. 6 in which the RW opening is located in the apical half (i.e., the vertical segment) of the RW membrane. The mean entry points through the RW and through a

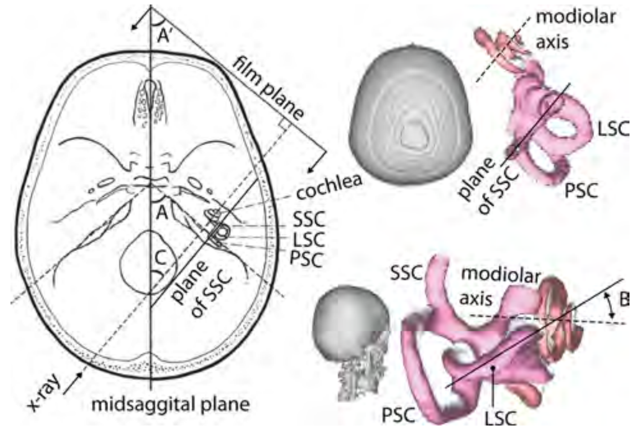

Fig. 4 The skull positioning of Fig. 2 was confirmed through more rigorous measurements using numerous temporal bones [12]. To confirm Fig. 2(*a*), they computed the angle *A* between the line passing the lower arm of the posterior semicircular canal (PSC) and the midsagittal plane, and assumed that *A* is nearly identical to *A*′ (left image). The mean value of *A* (for $n = 102$) is 52.5 deg. *C* is the complementary angle of *A* and is identical to θ_1 in Table 1 and Fig. 2. Next, to confirm Fig. 2(*b*), they computed the angle *B* between the lateral-semicircular canal (LSC) and the modiolar axis (bottom-right image). The mean value of *B* (for $n = 10$) is 28.2 deg. Since the LSC forms an angle of 30 deg upward from the infraorbitomeatal plane, they concluded that the modiolar axis is nearly parallel to this plane. Viewing the film plane in the direction indicated by the arrows results in the cochlear-view radiograph shown in Fig. 3. Modified left image is from Ref. [12] reproduced with permission of Wolters Kluwer Health. The right images are generated using software available for public use [15].

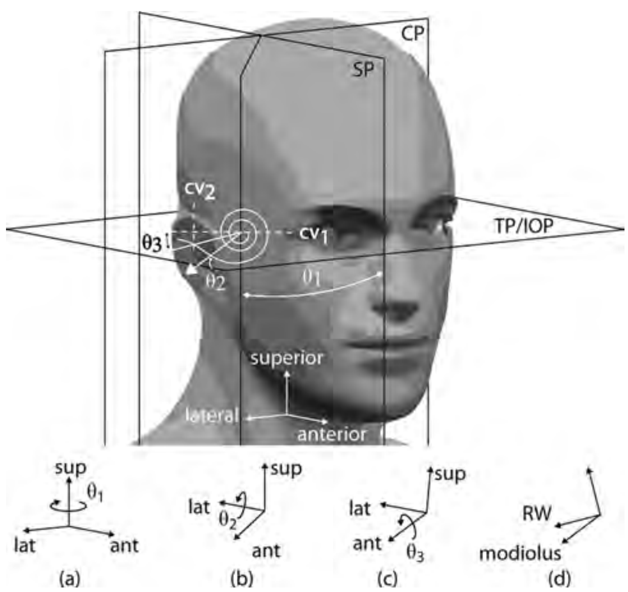

Fig. 5 Top: Orientation angles of Table 1 and cochlear-view axes (lines cv_1 and cv_2) are shown relative to the three orthogonal reference planes of the body: the sagittal plane (SP), coronal plane (CP), and the transverse plane (TP). θ_3 is measured in the plane formed by cv_1 and cv_2; modified public domain image. Bottom: cochlea orientation angles (shown as a series of successive rotations of a Cartesian frame originally aligned with the reference planes).

cochleostomy just apical of it are given as 13.5 deg (θ_3 in Table 1) and 23.8 deg, respectively, as measured in the plane of the basal cochlear turn from the 0 deg reference of the cochlear view [9]. The corresponding linear distances to these entry points are

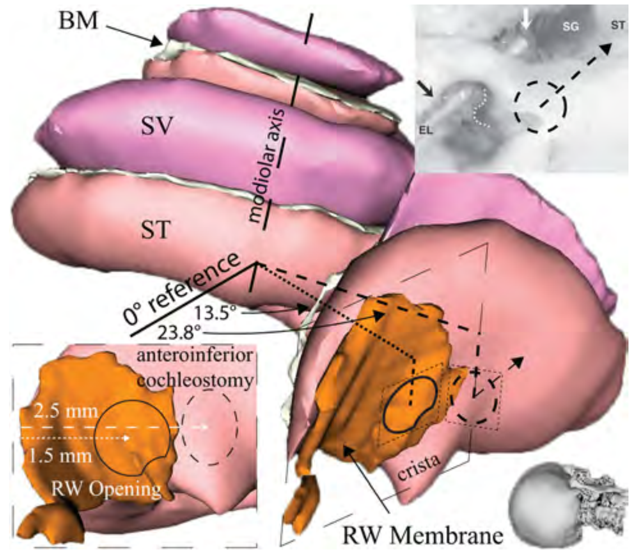

Fig. 6 Virtual model of the cochlea showing the basal end of the scala tympani (ST) as seen through the facial recess during surgery with an enlarged view of the RW region provided in the lower-left inset. Depictions of both insertion openings, RW opening and anteroinferior cochleostomy, are superimposed onto the virtual model to provide approximate locations with respect to the RW membrane. Basilar membrane (BM), scala vestibuli (SV), and the skull position corresponding to the cochlea orientation are provided for reference. Image is generated using software available for public use [15]. Top-right: posterior-superior lip of RW niche (black arrow) and bony projection from crista (outlined by dotted white line) restrict the angle of electrode (EL) entry so that the electrode tip (white arrow) is directed toward modiolar wall and spiral ganglion (SG) rather than the ST lumen. A well placed cochleostomy (shown as a dashed circle) can facilitate direct insertions into the ST lumen (dashed arrow). Modified image from Ref. [16] reproduced with permission of John Wiley and Sons.

approximately 1.5 mm and 2.5 mm as measured from the basal end of the ST. A virtual model of the cochlea, with approximate locations of the insertion holes, is shown in Fig. 6.

While a cochleostomy insertion can be replicated by a properly positioned hole, to model a RW insertion is more complicated due to the anatomy of the RW region. The RW membrane is recessed within a bony cavern called the RW niche (Fig. 7), which, in combination with the crista (i.e., the bony ridge adjacent to the RW membrane), restrict the entry angle such that the tip is directed toward the modiolar wall upon insertion [16] (top-right inset of Fig. 6). In extreme cases, where this interference prevents a compatible electrode path, reducing the posterior-superior lip of the RW niche and enlarging the opening at the anteroinferior margin will allow the surgeon to make insertions where the electrode is more aligned with the ST lumen. Since surgeons have the ability in practice to modify the anatomy for better visibility and access to the RW membrane [16,17], we assume that the surgeon has made the membrane accessible and replicate RW insertions by modeling only the incision into the RW membrane as an opening with a small protrusion near 5 o'clock to account for the obstruction due to the crista (bottom-left inset of Fig. 6).

Insertions through the RW are further complicated by a narrowing of the ST near the RW. This is illustrated in Fig. 7 as the cross-sectional width and height of the ST decrease toward the basal end of the RW. This narrowing is further exacerbated by a clockwise rotation of the osseous spiral lamina (OSL) from vertical at the posterior edge of the RW to more oblique angles deeper within the basal turn [18]. Thus, the initial trajectory of the electrode array is aligned with the short dimension of the ST rather than its long dimension. For example, at the middle of the RW

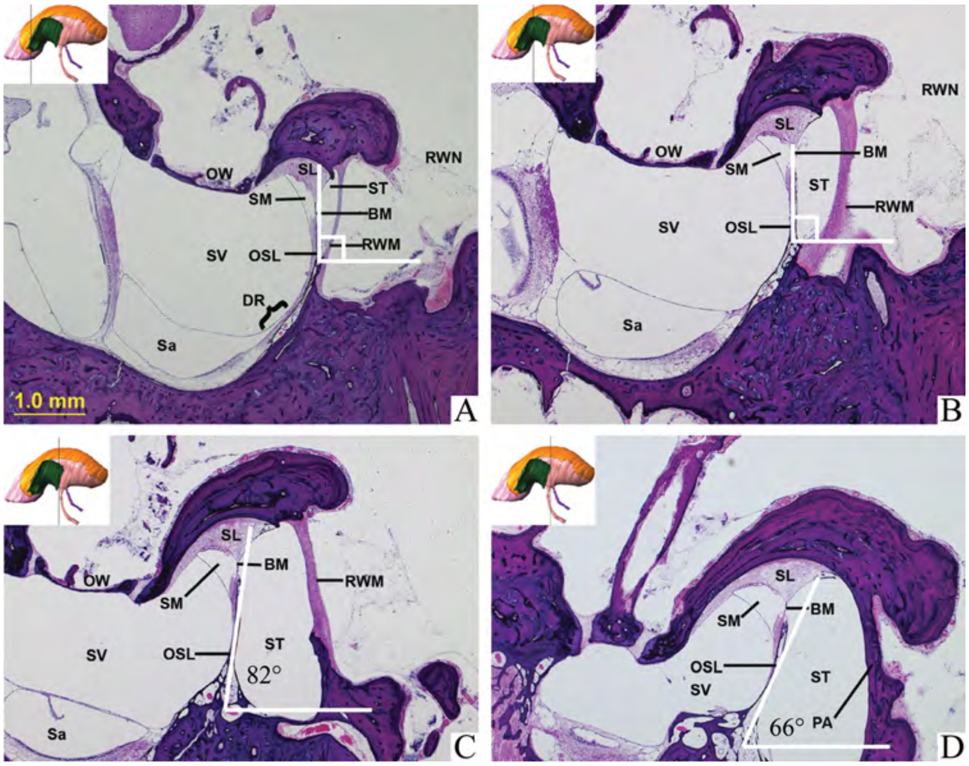

Fig. 7 Histological cross sections in the basal end of the cochlea. BM, basilar membrane; OSL, osseous spiral lamina; RWN, round-window niche; RWM, round-window membrane; SM, scala media; ST, scala tympani; SV, scala vestibuli. Modified images from Ref. [26] reproduced with permission of Lippincott Williams and Wilkins.

membrane, the long dimension of the ST has been effectively rotated away from the insertion direction such that the clearance between the inner wall of the ST and the electrode array tip upon insertion is only about 0.5 mm (Fig. 7(*b*)).

To model the narrowing of the RW region, we first note that the ST terminates near the RW [18], and assume that the basal end of the RW is near the beginning of the ST. Next, we approximate the RW membrane as a circle with a diameter of 2 mm, which is consistent with the dimensions reported by Nomura [19] and Erixon et al. [20]. Thus, the basal and apical end of the RW (Figs. 7(*a*) and 7(*c*)) corresponds to a distance of 0 mm and 2 mm, respectively, from the ST's beginning. With this, we can now align the various histological measurements, often given with respect to different reference markers [21–26].

Since detailed measurements of the OSL angle in the basal region of the cochlea are lacking in the available literature, we estimate this parameter by inspecting the OSL angle in the histology images found in Refs. [18,26] and with the software used to generate Fig. 6. (These estimates are listed in Table 3 as the ϕ values from $d = 0$ mm to $d = 5$ mm).

4 Consensus Cochlear Coordinates

To address the need to standardize CI insertion evaluations, a 3D cylindrical coordinate system, well suited for clinical measurements of CI insertions, was agreed upon by a panel of prominent researchers and manufacturers [9]. We adopt this coordinate system so that insertion experiments can be evaluated with the same metric as clinical insertions. A plane through the basal turn of the cochlea perpendicular to the modiolus is chosen as the plane of rotation. This is equivalent to the cochlear view, making this consensus framework straightforward to implement in our phantom. Angular measurements are measured from the center of the RW rather than the 0 deg reference of the cochlear view. The z-axis is placed through the center of the modiolus, with its origin at the level of the helicotrema (the apex of the cochlea). The radial distance from the modiolus to the implant completes the third component of the cylindrical coordinate system. Because our phantom is developed from a spiral model that computes radius and height as a function of angle (Eqs. (1)–(3)), the three coordinate values can be parameterized by a single angular measurement.

5 Construction of Scala-Tympani Phantom

5.1 Modeling the Scala Tympani. We now summarize the process to model the ST, which was originally described by Clark et al. [1]. The 3D spiral shape of the ST, expressed in cylindrical coordinates, can be described by the following equations:

$$R = C(1 - D\ln(\theta - \theta_0)) \qquad \theta < 100\,\text{deg} \tag{1}$$

$$R = A\mathrm{e}^{-B(0.0002\theta^2 + 0.98\theta)} \qquad \theta \geq 100\,\text{deg} \tag{2}$$

$$z = E(\theta - \theta_1) \tag{3}$$

R is the distance from the spiral center in mm, z is the height value in mm, and θ is the angle in degrees. Equations (1) and (2) are based on the spiral template of the cochlear view (Fig. 3). The values for constants A, B, C, D, E, θ_0, and θ_1 are listed in Table 2. We generate the spiral curve for a range of θ from 6.8 deg to 910.3 deg in 0.1 deg increments (Fig. 8).

Starting at the basal end of the spiral and at each 1 mm increment toward the apical end, we model the ST sections (Fig. 8) as

Table 2 Values for constants of equations (1), (2), and (3)

A (mm)	B (mm)	C (mm)	D (mm)	E (mm)	θ_0 (deg)	θ_1 (deg)
3.762	0.001317	7.967	0.1287	0.003056	5.0	10.3

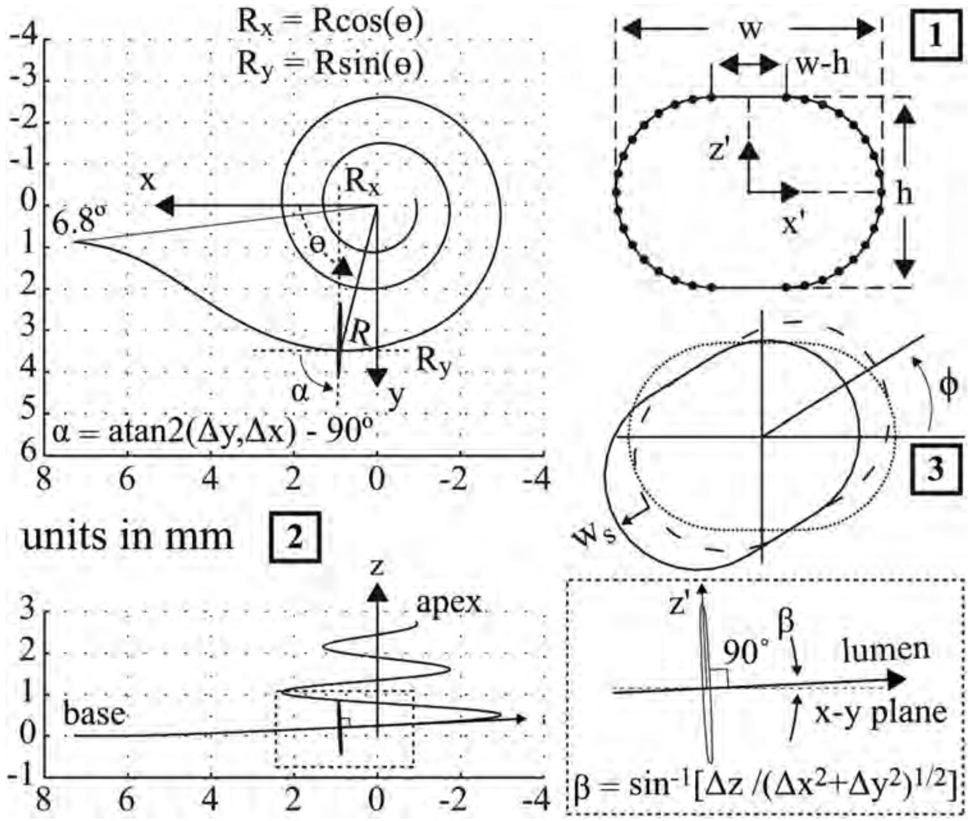

Fig. 8 Steps to model the scala tympani. (1) Create sections parameterized by *h* and *w*. (2) Place the origin of each section (intersection of x' and z') onto the spiral at 1 mm increments from its beginning, with z' initially aligned with z, and orient the section such that it is orthogonal to the local spiral direction. (3) Rotate section counterclockwise by ϕ and shift section medially by w_s.

semicircular ends, connected by straight segments, parameterized by width and height values given in Table 3. The ST width and height from the previous phantom [1] were taken from Wysocki's mean width and height measurements of 25 temporal bones taken at 1 mm increments from the ST's beginning [21]. However, the ST height seemed undersized based on our experience. This is confirmed by comparing Wysocki's data against other published data [22–25] (Fig. 9). Since, in our opinion, this discrepancy indicates a systemic error with Wysocki's data, we averaged the height data from the other publications and use this for the ST height values instead. We also confirmed that no change was needed for the ST width as Wysocki's width measurements were consistent with the other data sets. Each section is oriented so that it is orthogonal to the lumen, rotated by ϕ to model the OSL angle, and shifted medially by w_s (Fig. 8) to better match Cohen's silastic models [11] and Kawano's reconstructions [27] (Fig. 10).

We note that the section at 0 mm in Ref. [1] is equivalent to the section at 2 mm here. The reason is that previously the first two cross sections were ignored, shortening the overall length of the ST and widening the phantom's opening. To include these initial cross sections, we extend the starting point of the spiral template from 10.3 deg to 6.8 deg. The previous starting point (10.3 deg) was used to approximate the basal end of the organ of Corti [28]. More recently, some have concluded that the actual basal end of the organ of Corti is likely closer to 5 deg than to 10 deg, which would indicate an earlier start angle [9]. Moreover, by lengthening the basal end of the spiral, the angular locations of the RW opening and cochleostomy are better matched to the appropriate linear distances from the basal end (see Fig. 6 inset). That is, the locations of the RW opening and the cochleostomy (the intersections of our ST's outer wall with 13.5 deg and 23.8 deg lines, respectively) should be about 1.5 mm and 2.5 mm, respectively, from the basal end (Fig. 11). Finally, the values for ϕ at 6 and 7 mm are interpolated to provide a smooth transition from the estimated OSL values to the values originally determined by Clark et al. from 8 mm on.

5.2 Phantom Design and Fabrication. The phantom design based on the modeled ST is illustrated in Fig. 12 and is based on the process detailed by Clark et al. [1]. Our phantom is designed such that if placed on a tabletop, the ST's orientation matches the values in Table 1. The angular grid is designed with the 0 deg reference through the center of the RW. An exit hole is placed at the top of the phantom to allow for fluid to travel through the cavity.

We model the cochleostomy opening as a 1.2 mm diameter hole centered near the intersection of the 23.8 deg line with the outer boundary of our modeled ST. Since the primary feature of a cochleostomy insertion is an initial electrode trajectory in line with the ST lumen (i.e., the longitudinal axis of the ST) [18], we orient the opening toward the lumen. The size of the opening is somewhat arbitrary as it will depend on surgeon preference and manufacturer recommendations. For example, a survey of surgeons resulted in a preferred cochleostomy range between 0.8 and 2.0 mm [29].

Similarly, the RW opening is a 1.2 mm diameter hole centered near the intersection of the 13.5 deg line with the outer boundary of our modeled ST. Since the phantom is essentially a solid structure with a cavity representing the ST, the insertion openings will have a tunnel effect due to the material wall thickness at the opening. This effect is an artifact of the design, and is not an inherent characteristic of the surgical insertion. To minimize this effect for RW insertions, we trim material to the boundary of the cavity (shown as a red dashed line in Fig. 12) to a wall thickness of

0.3 mm. This is not necessary for cochleostomy insertions since this artifact does not affect the initial electrode trajectory. Finally, a small protrusion near 5 o'clock is added to the RW opening to account for the obstruction due to the crista.

A usable phantom requires it to be transparent enough to visualize the implant during insertions and have a smooth internal surface to mimic the endosteum lining of the ST [6]. A multistep casting process, such as that used in the investment casting of jewelry, has been successfully used to produce transparent cochlea models [7]. However, the complexity of this multistep process is not ideal where only a few phantoms are desired. A simpler method is to 3D print the device directly from software.

We now note some limitations with 3D printing that affect the usability of this device. First, not all additive manufacturing processes can build with transparent materials. Second, the layer-by-layer building operations inherent in these processes leave a stair-step finish. Thus, the smoothness of the surface is limited by the resolution of the build layers. Third, designs with complex geometries, such as overhangs and tunnels often require the deposition of support material to act as a temporary scaffold while these features are built. In the case of our phantom, removal of this temporary support structure from within the internal cavity is difficult. Fourth, a nonsmooth surface finish usually results where the temporary support structure contacts the actual build material. Surface polishing, often used to smooth out these aforementioned features, is not a viable option since the internal channel is not easily accessible. It is conceivable that continual advancements in 3D printing technology will render these concerns obsolete in the future. For now, the best results are achieved by high-resolution machines that can build complex geometries with minimal, easily removable, support material.

We produced two sets of phantoms using the machines in Table 4. The Viper si2 SLA is a high-definition stereolithography machine capable of building in transparent plastic (Watershed XC11122) without requiring any support material, eliminating the problem of support-material removal from the internal cavity. The next generation of microstereolithography machines is capable of better resolutions and accuracies, but at this time is not widely available. The ProJet HD 3000*Plus*, operated in Xtreme high definition (XHD) mode, has the best resolution and accuracy in its class. The support material is completely meltable, allowing for hands-free removal of the build-support structures. The primary negative is that a transparent material is currently not available for use with this printer, which is not ideal for visualizing insertions. The SOLIDWORKS (Waltham, MA) renderings and the manufactured phantoms are shown in Fig. 13 with a MED-EL (Innsbruck, Austria) standard electrode inserted into them.

To account for the machine's resolution and accuracy, we recommend an enlarged ST channel to minimize the possibility that an undersized channel is produced. This adjustment seems reasonable given that an undersized ST will unnecessarily hinder insertion experiments. Rebscher et al. oversized the ST cavity in their ST model by 14% for this specific reason [7]. For a 1 mm × 2 mm cross section, this amounts to 0.14 mm to 0.28 mm. For perspective, the average of published standard deviations is about 0.14 mm [21–24]. Our ST prototypes are oversized by 0.14 mm in both width and height beyond the values given in Table 3.

5.3 Validation. We validate the usefulness of our phantoms through insertion experiments similar to those described in Ref. [2]. To automate the insertions, standard MED-EL electrodes are mounted to a Thorlabs (Newton, NJ) MTS50/M-Z8 linear stage. By rigidly mounting the phantoms onto an ATI (Apex, NC) Nano17, six-axis, force-torque sensor (3.125 mN resolution), forces on the phantoms can be measured during automated insertions. Prior to each insertion, the channel is filled with saline solution and the electrode tip is positioned just inside the opening.

The first set of experiments compares our cochleostomy phantom with the cochleostomy phantoms available through the three

Table 3 Values for the independent parameters (shown in Fig. 8) used to generate and locate the ST sections. *d* is the distance along the spiral from its beginning at $\theta = 6.83$ deg. *h* and *w* are the ST height and width, respectively, ϕ is the osseous spiral lamina angle, and w_s is the distance to shift the sections medially.

d (mm)	0	1	2	2.5	3	4	5	6	7	8	9	10	11	12	13	14	15	16	17
θ (deg)	6.8	9.5	15.1	19.0	23.5	34.3	46.7	60.4	75.3	91.3	108.4	126.1	144.2	162.8	181.9	201.5	221.6	242.4	263.7
h (mm)	0.3	0.6	1.30	1.58	1.53	1.36	1.33	1.28	1.27	1.26	1.22	1.18	1.14	1.10	1.07	1.03	1.00	0.97	0.96
w (mm)	0.7	1.5	2.10	2.10	2.10	1.95	1.85	1.80	1.74	1.70	1.68	1.63	1.60	1.59	1.51	1.50	1.54	1.46	1.45
ϕ (rad)	1.57	1.57	1.43	1.17	0.97	0.56	0.00	0.02	0.04	0.06	0.07	0.08	0.09	0.10	0.11	0.12	0.13	0.14	0.15
w_s (mm)	0.0	0.0	0.0	0.0	0.0	0.0	0.3	0.3	0.28	0.26	0.24	0.28	0.28	0.32	0.35	0.4	0.5	0.55	0.62
d (mm)	18	19	20	21	22	23	24	25	26	27	28	29	30	31	32	33	34	35	36
θ (deg)	285.8	308.5	332.0	356.4	381.6	407.8	435.1	463.6	493.4	524.6	557.3	591.9	628.4	667.2	708.6	753.0	800.9	853.0	910.1
h (mm)	0.93	0.92	0.92	0.92	0.91	0.91	0.92	0.94	0.93	0.89	0.82	0.76	0.73	0.77	0.73	0.70	0.65	0.67	0.58
w (mm)	1.43	1.38	1.33	1.32	1.31	1.30	1.30	1.30	1.30	1.30	1.30	1.30	1.31	1.31	1.26	1.15	1.23	1.25	1.45
ϕ (rad)	0.16	0.17	0.18	0.19	0.20	0.21	0.22	0.23	0.24	0.25	0.26	0.27	0.28	0.29	0.30	0.25	0.20	0.15	0.10
w_s (mm)	0.62	0.6	0.6	0.65	0.66	0.67	0.68	0.65	0.65	0.65	0.57	0.49	0.41	0.33	0.25	0.17	0.09	0.01	0.01

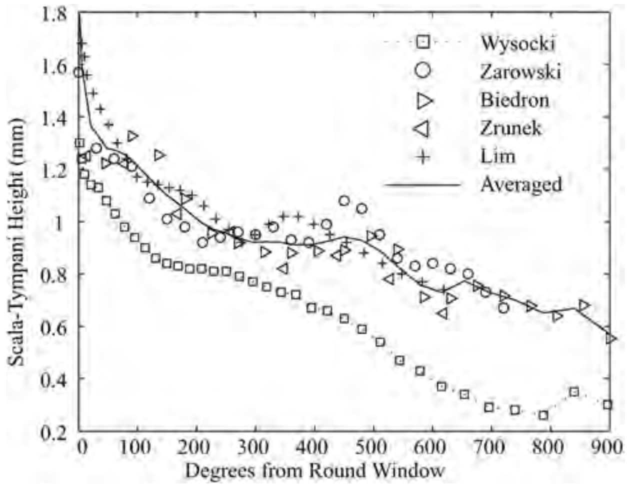

Fig. 9 Wysocki's height data [21] is smaller than other published values [22–25]. The solid line is the average of the non-Wysocki data sets.

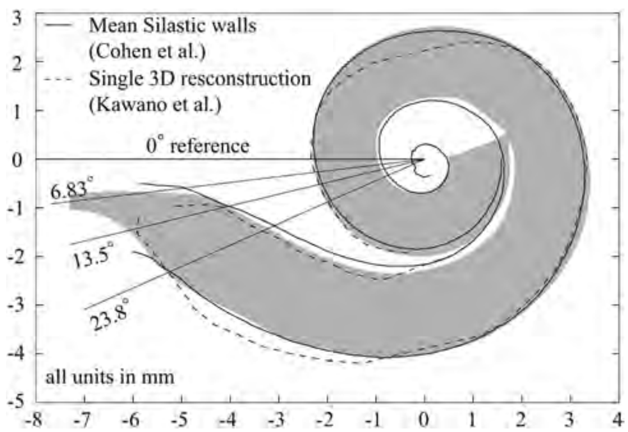

Fig. 10 Our scala-tympani model (shown in gray and limited to 1.5 turns to reduce visual clutter) is compared with Cohen's silastic models [11] and Kawano's reconstructions [27]. The intersections of the outer wall of our model with the 13.5 deg and 23.8 deg lines are the respective entry points through the round-window opening and an anteroinferior cochleostomy. Modified image from Ref. [9] reproduced with permission of Wolters Kluwer Health.

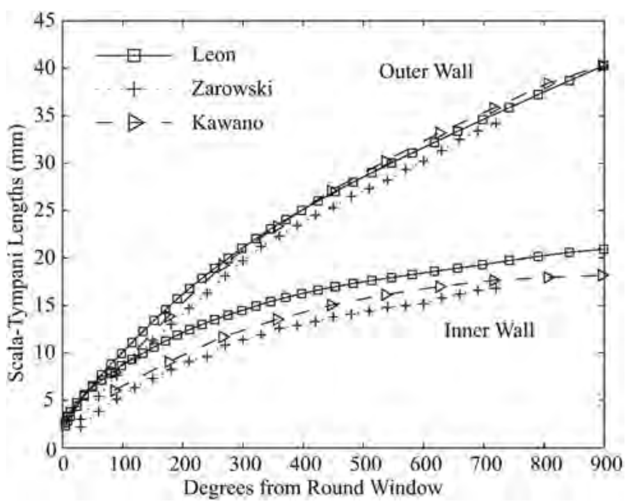

Fig. 11 Our scala-tympani wall lengths compared with published data [22,27]

Table 4 Machines used to build prototypes of Fig. 13

3D Systems (Rock Hill, SC)	ProJet HD 3000*Plus*	Viper si2 SLA
Layer thickness (μm)	16 (XHD Mode)	51 (Hi Res Mode)
Accuracy (μm)	25–50	127
Material	VisiJet Crystal	Watershed XC11122

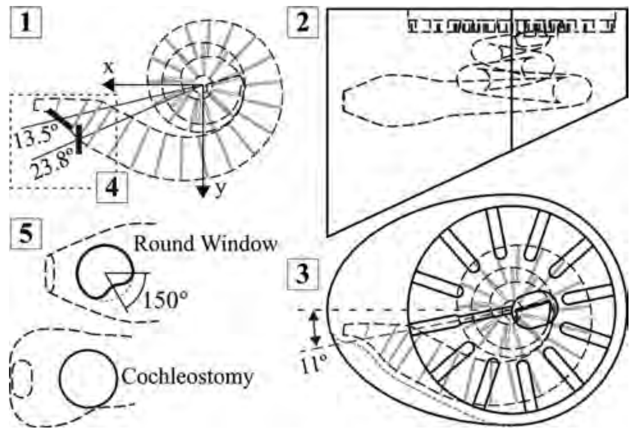

Fig. 12 Steps to design phantom in SolidWorks. (1) Create loft from imported *x-y-z* points that model the scala tympani. (2) Build a structure around the lofted cut to orient the phantom appropriately. (3) Create the angular grid system and an exit hole near center of the dial. For the round-window version, we trim material along the cavity boundary (red-dashed line) to reduce the tunnel effect from the phantom's wall thickness at the round-window opening. (4) Create sketch planes where the 13.5 deg and 23.8 deg lines intersect the lofted cut. (5) Create insertion openings on the defined sketch planes.

major CI device manufacturers (Fig. 14). The version from Advanced Bionics is made through a multistep casting process, but it models all three scala chambers as a single cavity. This overstates the channel size that the electrode travels through and makes insertions easier, which is especially evident for deeper insertions.

The version by MED-EL is made using stereolithography and has the shortest section between the opening and the basal turn. Thus, in the MED-EL model, electrodes travel a shorter distance to reach the same angular insertion depth as compared with the others and have the effect of overstating the insertion forces at deeper insertions.

The version by Cochlear (Sydney, Australia) is only a planar model. That is, it does not replicate a full 3D path for the electrode to travel through. The measured insertion forces are between the lower and upper bound set by Advanced Bionics and MED-EL, respectively.

The two versions of our cochleostomy phantoms are identified as numbers 4 and 5 in Fig. 14. Phantom 4 performed similarly to the version by Cochlear and phantom 5 resulted in lower insertion forces than phantom 4. This suggests that the ProJet HD 3000*Plus* produces a device with a smoother internal surface finish than that made by the Viper si2 SLA. This is consistent with the stated machine resolution and accuracy tolerances provided by manufacturer (Table 4). A significant disadvantage of the ProJet HD 3000*Plus* is that the material is only semitransparent and does not provide good visualization of an electrode inside it. Since both devices perform comparably with those widely in use, we recommend using the version made with the completely transparent plastic.

The second set of experiments compares our RW phantom with cadaver cochleae to determine if insertion force experiments conducted in our device can be a reliable indicator of insertion force measurements in an actual cadaver cochlea (Fig. 15). Unlike the

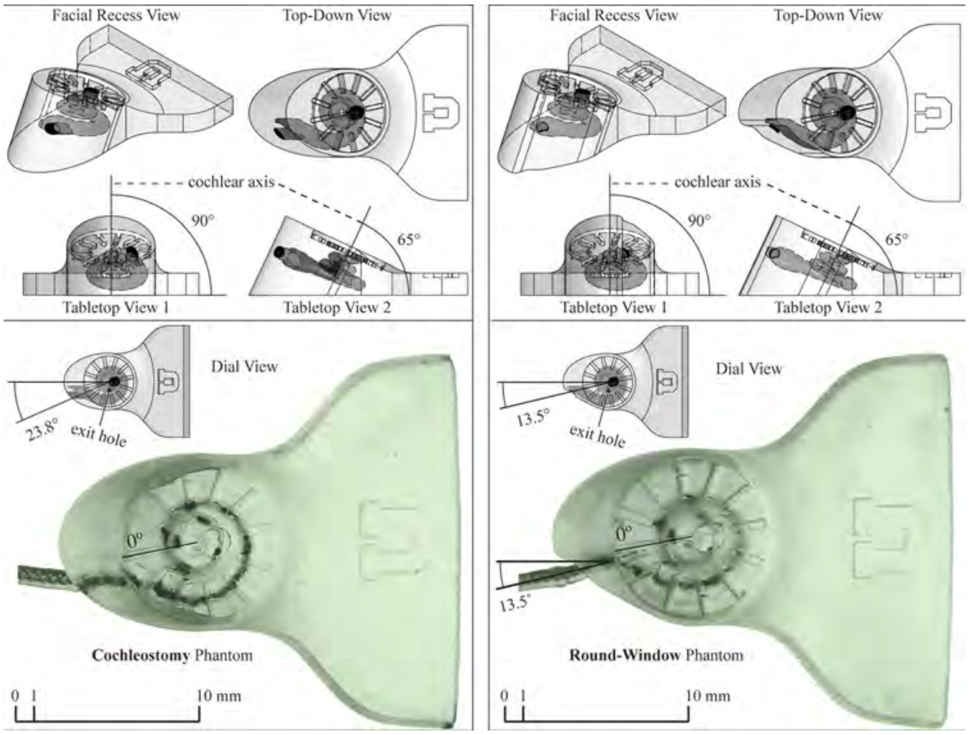

Fig. 13 SolidWorks renderings of the cochleostomy (top-left) and round-window (top-right) versions of our scala-tympani phantom are used to manufacture the corresponding devices below. The tabletop views assume the phantom is lying on a flat surface with the observer's line-of-sight at the level of the phantom. The facial recess views approximate the surgeon's view of the insertion openings, in the spirit of Fig. 6. The top-down views are taken above the phantom with the line-of-sight along the gravity vector. The dial views assume a line-of-sight directed toward and orthogonal to the face of the dial. Standard MED-EL electrodes are inserted as far as possible before buckling (to approximately 720 deg) into both phantoms.

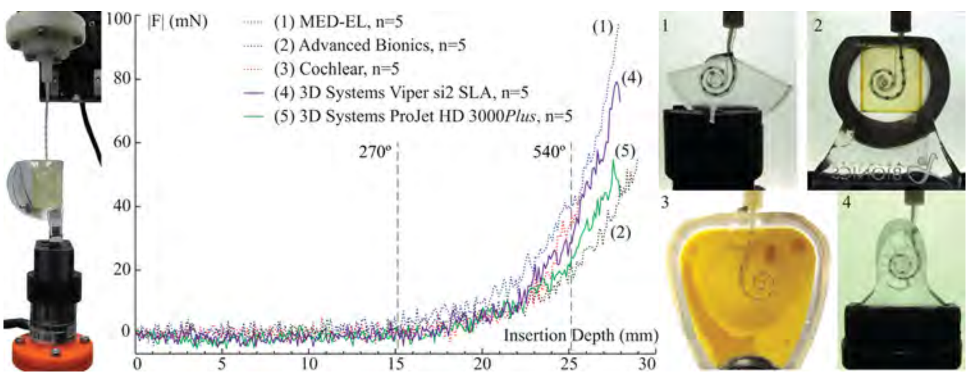

Fig. 14 Insertion force measurements are compared for five different phantoms, each of which is rigidly mounted onto a force sensor with the insertion opening oriented for vertical, automated insertions. An image of phantom number 5 is not provided because its semitransparent material did not provide good visualization of the electrode.

first set of experiments, the automated insertions are not conducted vertically but at an orientation that replicates actual surgical insertions. Bone sections containing the cochleae are dissected out of two temporal bones chosen randomly from the University of Utah Temporal Bone Lab and fixed with paraffin wax in a basket that is rigidly mounted to the force sensor. We carefully open the RW membrane, fill the cochleae with saline solution, and position the electrode with its tip just inside the RW. We conduct one automated insertion into each cadaver cochlea and stop the insertion if buckling occurs to protect the electrode array from permanent damage.

The measured forces are very similar between the cadaver cochleae and the RW phantom. A deeper insertion was achieved with cadaver cochlea 1 than with cadaver cochlea 2. Since the cadaver cochleae are not transparent, it is possible that the insertion stage was slightly misaligned relative to the ST hindering a full insertion. Although the number of cochleae was limited to two, they were chosen randomly, indicating that, in our opinion, insertion forces measured in our RW phantom can be used as an indicator of actual measurements in a cadaver cochlea.

6 Discussion

The orientation of our phantom is largely based on mean values of the required skull orientation angles to produce a radiographic image that is orthogonal to the cochlear axis and parallel to the plane of the basal cochlear turn. Although we have chosen to

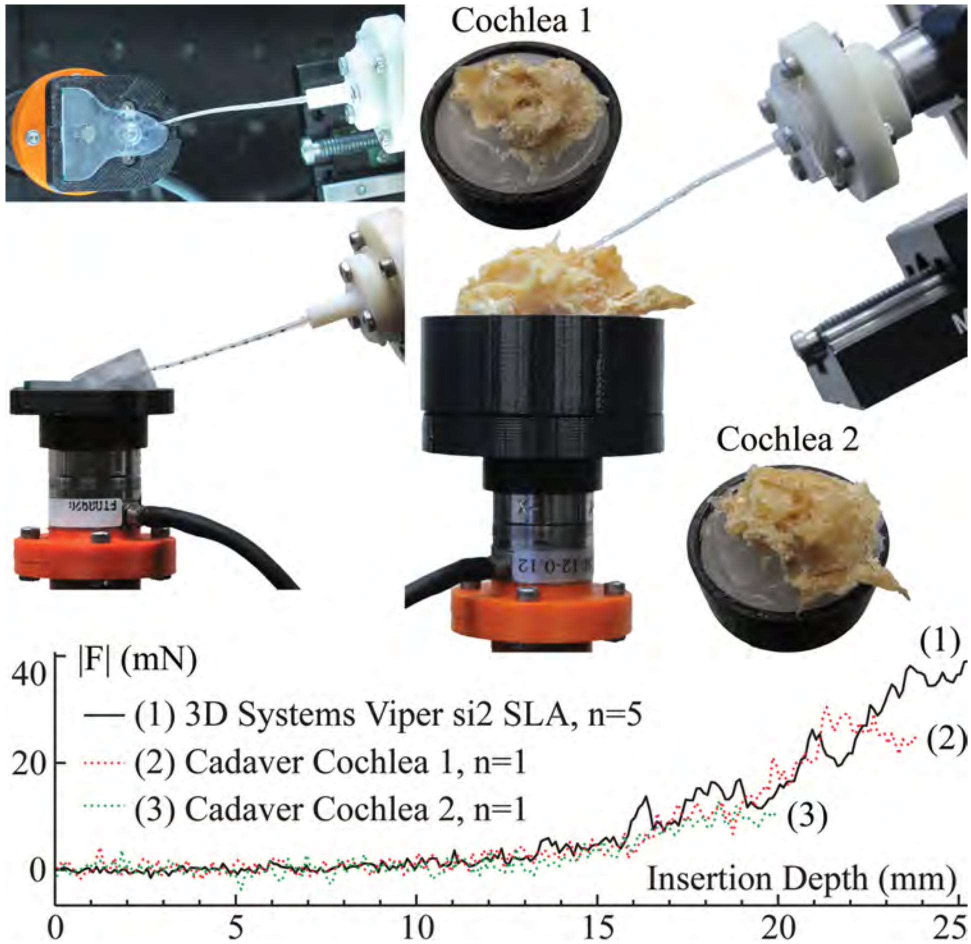

Fig. 15 Insertion force measurements, at clinically accurate insertion angles, are compared between the round-window phantom (left) and cadaver cochleae fixed in baskets with paraffin wax (right), mounted rigidly to the force sensor

incorporate the findings associated with the cochlear view, a different group, also interested in radiologic evaluations of CI insertions, published a different set of skull orientation angles ($\theta_1 = 30$ deg, $\theta_2 = 15$ deg) [30]. They do not, however, provide the location of the RW in their findings, which is a key feature of this phantom. Furthermore, the cochlear view appears to have gained larger clinical acceptance.

To orient the phantom with respect to the tabletop, two key assumptions were made. First, the infraorbitomeatal lines are determined by anatomical landmarks that are set in the patient's skull and will vary from patient to patient. We assume that these lines are parallel to the transverse plane since typically they are nearly horizontal [12]. Second, we assume that axis 2 of the cv_2 lies in the plane of the superior-semicircular canal, allowing us to regard θ_3 with respect to a plane parallel to the infraorbitomeatal plane. This simplifies the orientation of the phantom on a tabletop and is within the listed variability (Table 1).

Our phantom models an anteroinferior cochleostomy, but there is not complete consensus regarding the cochleostomy site through which CI insertions are least traumatic to the delicate intracochlear structures. Most seem to prefer an anteroinferior cochleostomy [8,26,29,31,32], though a cochleostomy that is mostly inferior [18] or mostly anterior [33] to the RW have their proponents. Still others involve the RW membrane itself into the cochleostomy [34]. Regardless, the ideal cochleostomy will facilitate electrode insertions with an insertion trajectory in line with the ST lumen, which we model in our phantom.

Insertions through the RW are actually more complicated than what has been modeled in our phantom because the RW membrane is recessed into a complex, cavernous structure (the RW niche) that limits visibility and access to the membrane. Rather than model the complex niche, which has been attempted [19], we assume that the surgeon has made the membrane accessible and simply model an incision into the RW membrane. Neglecting the niche simplifies the phantom model and is reasonable given that the surgeon has the ability in practice to remove portions of the niche for better visibility and access to the RW membrane [16,17]. That said, our model can be easily reconfigured to simulate the niche by setting the wall thickness at the RW to the measured depth of the niche [35].

Additionally, this phantom does not replicate the access limitations of the facial recess. This is true of all insertion experiments that use either cochlea models or cadaver cochleae that have been dissected out of temporal bones.

An angular grid has been designed into the phantom to accommodate the industry's movement toward standardization. As an added benefit, angular measurements can be interpreted in the context of the cochlea's tonotopic arrangement. That is, the electrode position given as an angular location from the RW can be used to determine the frequencies communicated to the cochlea. Furthermore, a metric of the proximity of the electrode position to the modiolus (to evaluate the effectiveness of modiolus-hugging designs) can be computed by dividing the angular insertion depth by the linear insertion depth [32].

7 Conclusions

A scala-tympani phantom for cochlear-implant insertions through the round-window or a cochleostomy has been presented.

It is primarily aimed at those performing insertion experiments but can also be used as part of an insertion simulation for training or education. More information about these phantoms, including SOLIDWORKS and MATLAB files, can be obtained from the University of Utah's Telerobotics Lab (www.telerobotics.utah.edu).

Acknowledgment

This material is based upon work supported by the National Science Foundation under Grant Nos. 0952718 and 0654414. We would like to thank Brian M. Chin, M.D. (Neuroradiology Fellow at the University of Utah School of Medicine) for his assistance in understanding skull positions of the Cochlear View. We also would like to thank Abhijit Kulkarni, Ph.D. and Kurt Koester, Ph.D. (Advanced Bionics) for insight regarding manufacturing of cochlea models. MED-EL electrode arrays and a MED-EL scala-tympani phantom were provided courtesy of Claude Jolly, Ph.D. and Mr. Anandhan Dhanasingh (MED-EL).

References

[1] Clark, J. R., Warren, F. M., and Abbott, J. J., 2011, "A Scalable Model for Human Scala-Tympani Phantoms," ASME J. Med. Dev., **5**(1), p. 014501.

[2] Clark, J. R., Leon, L., Warren, F. M., and Abbott, J. J., 2012, "Magnetic Guidance of Cochlear Implants: Proof-of-Concept and Initial Feasibility Study," ASME J. Med. Dev., **6**(3), p. 035002.

[3] Zhang, J., Wei, W., Ding, J., Roland, J. T., Jr., Manolidis, S., and Simaan, N., 2010, "Inroads Toward Robot-Assisted Cochlear Implant Surgery Using Steerable Electrode Arrays," Otol. Neurotol., **31**(8), pp. 1199–1206.

[4] Majdani, O., Schurzig, D., Hussong, A., Rau, T., Wittkopf, J., Lenarz, T., and Labadie, R. F., 2010, "Force Measurement of Insertion of Cochlear Implant Electrode Arrays In Vitro: Comparison of Surgeon to Automated Insertion Tool," Acta Otolaryngol., **130**(1), pp. 31–36.

[5] Verbist, B. M., Joemai, R. M. S., Teeuwisse, W. M., Veldkamp, W. J. H., Geleijns, J., and Frijns, J. H. M., 2008, "Evaluation of 4 Multisection CT Systems in Postoperative Imaging of a Cochlear Implant: A Human Cadaver and Phantom Study," Am. J. Neuroradiol., **29**(7), pp. 1382–1388.

[6] Todd, C. A., Naghdy, F., and Svehla, M. J., 2007, "Force Application During Cochlear Implant Insertion: An Analysis for Improvement of Surgeon Technique," IEEE Trans. Biomed. Eng., **54**(7), pp. 1247–1255.

[7] Rebscher, S. J., Talbot, N., Bruszewski, W., Heilmann, M., Brasell, J., and Merzenich, M. M., 1996, "A Transparent Model of the Human Scala Tympani Cavity," J. Neurosci. Methods, **64**(1), pp. 105–114.

[8] Rebscher, S. J., Hetherington, A., Bonham, B., Wardrop, P., Whinney, D., and Leake, P. A., 2008, "Considerations for Design of Future Cochlear Implant Electrode Arrays: Electrode Array Stiffness, Size, and Depth of Insertion," J. Rehabil. Res. Dev., **45**(5), pp. 731–747.

[9] Verbist, B. M., Skinner, M. W., Cohen, L. T., Leake, P. A., James, C., Boëx, C., Holden, T. A., Finley, C. C., Roland, P. S., Roland, J. T., Jr., Haller, M., Patrick, J. F., Jolly, C. N., Faltys, M. A., Briaire, J. J., and Frijns, J. H. M., 2010, "Consensus Panel on a Cochlear Coordinate System Applicable in Histologic, Physiologic, and Radiologic Studies of the Human Cochlea," Otol. Neurotol., **31**(5), pp. 722–730.

[10] Marsh, M. A., Xu, J., Blamey, P. J., Whitford, L. A., Xu, S. A., Silverman, J. M., and Clark, G. M., 1993, "Radiologic Evaluation of Multichannel Intracochlear Implant Insertion Depth," Am. J. Otol., **14**(4), pp. 386–391.

[11] Cohen, L. T., Xu, J., Xu, S. A., and Clark, G. M., 1996, "Improved and Simplified Methods for Specifying Positions of the Electrode Bands of a Cochlear Implant Array," Am. J. Otol., **17**(6), pp. 859–865.

[12] Xu, J., Xu, S. A., Cohen, L. T., and Clark, G. M., 2000, "Cochlear View: Postoperative Radiography for Cochlear Implantation," Am. J. Otol., **21**(1), pp. 49–56.

[13] Skinner, M. W., Holden, T. A., Whiting, B. R., Voie, A. H., Brunsden, B., Neely, J. G., Saxon, E. A., Hullar, T. E., and Finley, C. C., 2007, "In Vivo Estimates of the Position of Advanced Bionics Electrode Arrays in the Human Cochlea," Ann. Otol. Rhinol. Laryngol. Suppl., **116**(4), pp. 2–24.

[14] Verbist, B. M., Joemai, R. M., Briaire, J. J., Teeuwisse, W. M., Veldkamp, W. J., and Frijns, J. H., 2010, "Cochlear Coordinates in Regard to Cochlear Implantation: A Clinically Individually Applicable 3 Dimensional CT-Based Method," Otol. Neurotol., **31**(5), pp. 738–744.

[15] Wang, H., Northrop, C., Burgess, B., Liberman, M. C., and Merchant, S. N., 2006, "Three-Dimensional Virtual Model of the Human Temporal Bone: A Stand-Alone, Downloadable Teaching Tool," Otol. Neurotol., **27**(4), pp. 452–457.

[16] Roland, P. S., Wright, C. G., and Isaacson, B., 2007, "Cochlear Implant Electrode Insertion: The Round Window Revisited," Laryngoscope, **117**(8), pp. 1397–1402.

[17] Lenarz, T., Stover, T., Buechner, A., Paasche, G., Briggs, R., Risi, F., Pesch, J., and Battmer, R.-D., 2006, "Temporal Bone Results and Hearing Preservation With a New Straight Electrode," Audiol. Neurotol., **11**(Suppl. 1), pp. 34–41.

[18] Briggs, R. J. S., Tykocinski, M., Stidham, K., and Roberson, J. B., 2005, "Cochleostomy Site: Implications for Electrode Placement and Hearing Preservation," Acta Otolaryngol., **125**(8), pp. 870–876.

[19] Nomura, Y., 1984, "Otological Significance of the Round Window," Adv. Otorhinolaryngol., **33**, pp. 1–162.

[20] Erixon, E., Högstorp, H., Wadin, K., and Rask-Andersen, H., 2009, "Variational Anatomy of the Human Cochlea: Implications for Cochlear Implantation," Otol. Neurotol., **30**(1), pp. 14–22.

[21] Wysocki, J., 1999, "Dimensions of the Human Vestibular and Tympanic Scalae," Hear. Res., **135**(1–2), pp. 39–46.

[22] Zarowski, A., Offeciers, E., Postnov, A., Vanpoucke, F., and Peeters, S., 2008, "Micro-CT Anatomical Measurements in the Human Cochlea," *Auditory Research Bulletin 2007 Biennial Edition*, Advanced Bionics LLC, Valencia, CA.

[23] Biedron, S., Prescher, A., Ilgner, J., and Westhofen, M., 2010, "The Internal Dimensions of the Cochlear Scalae With Special Reference to Cochlear Electrode Insertion Trauma," Otol. Neurotol., **31**(5), pp. 731–737.

[24] Zrunek, M., Lischka, M., Hochmair-Desoyer, I., and Burian, K., 1980, "Dimensions of the Scala Tympani in Relation to the Diameters of Multichannel Electrodes," Eur. Arch. Otorhinolaryngol., **229**(3–4), pp. 159–165.

[25] Lim, Y. S., Park, S.-I., Kim, Y. H., Oh, S. H., and Kim, S. J., 2005, "Three-Dimensional Analysis of Electrode Behavior in a Human Cochlear Model," Med. Eng. Phys., **27**(8), pp. 695–703.

[26] Li, P. M. M. C., Wang, H., Northrop, C., Merchant, S. N., and Nadol, J. B., Jr., 2007, "Anatomy of the Round Window and Hook Region of the Cochlea With Implications for Cochlear Implantation and Other Endocochlear Surgical Procedures," Otol. Neurotol., **28**(5), pp. 641–648.

[27] Kawano, A., Seldon, H. L., and Clark, G. M., 1996, "Computer-Aided Three-Dimensional Reconstruction in Human Cochlear Maps: Measurement of the Lengths of Organ of Corti, Outer Wall, Inner Wall, and Rosenthal's Canal," Ann. Otol. Rhinol. Laryngol., **105**(9), pp. 701–709.

[28] Yoo, S. K., Wang, G., Rubinstein, J. T., Skinner, M. W., and Vannier, M. W., 2000, "Three-Dimensional Modeling and Visualization of the Cochlea on the Internet," IEEE Trans. Inf. Technol. Biomed., **4**(2), pp. 144–151.

[29] O'Connor, E. F., and Fitzgerald, A., 2010, "Hearing Preservation Surgery: Current Opinions," Adv. Otorhinolaryngol., **67**, pp. 108–115.

[30] Czerny, C., Steiner, E., Gstoettner, W., Baumgartner, W. D., and Imhof, H., 1997, "Postoperative Radiographic Assessment of the Combi 40 Cochlear Implant," Am. J. Roentgenol., **169**(6), pp. 1689–1694.

[31] Adunka, O. F., and Buchman, C. A., 2007, "Scala Tympani Cochleostomy I: Results of a Survey," Laryngoscope, **117**(12), pp. 2187–2194.

[32] Wardrop, P., Whinney, D., Rebscher, S. J., Luxford, W., and Leake, P., 2005, "A Temporal Bone Study of Insertion Trauma and Intracochlear Position of Cochlear Implant Electrodes. II: Comparison of Spiral Clarion and HiFocus II Electrodes," Hear. Res., **203**(1–2), pp. 68–79.

[33] Boyd, P. J., 2011, "Potential Benefits From Deeply Inserted Cochlear Implant Electrodes," Ear Hear., **32**(4), pp. 411–427.

[34] Majdani, O., Rau, T. S., Baron, S., Eilers, H., Baier, C., Heimann, B., Ortmaier, T., Bartling, S., Lenarz, T., and Leinung, M., 2009, "A Robot-Guided Minimally Invasive Approach for Cochlear Implant Surgery: Preliminary Results of a Temporal Bone Study," Int. J. Comput. Assist. Radiol. Surg., **4**(5), pp. 475–486.

[35] Su, W.-Y., Marion, M. S., Hinojosa, R., and Matz, G. J., 1982, "Anatomical Measurements of the Cochlear Aqueduct, Round Window Membrane, Round Window Niche, and Facial Recess," Laryngoscope, **92**(5), pp. 483–486.